DEM Simulation of a 3D Vertical Vibratory Screening Process: The Study of a Simulated Woven-Mesh Structure

Kuo Lun Tung
Dept. of Chemical Engineering, Chung Yuan Christian University, Chungli 320, Taiwan, R.O.C

R&D Center for Membrane Technology, Chung Yuan Christian University, Chungli 320, Taiwan, R.O.C

Ting Hsiang Chang
Dept. of Chemical Engineering, Chung Yuan Christian University, Chungli 320, Taiwan, R.O.C

Yi-Feng Lin
Dept. of Chemical Engineering, Chung Yuan Christian University, Chungli 320, Taiwan, R.O.C

R&D Center for Membrane Technology, Chung Yuan Christian University, Chungli 320, Taiwan, R.O.C

Chien-Song Chyang
Dept. of Chemical Engineering, Chung Yuan Christian University, Chungli 320, Taiwan, R.O.C

DOI 10.1002/aic.12311
Published online June 16, 2010 in Wiley Online Library (wileyonlinelibrary.com).

A discrete-element method (DEM) was applied to analyze the complicated phenomena of granular screening using different plate-, bead-, and woven-mesh structures. In the past, mesh structures have often been simplified as plate or bead structures in screening-process simulations, resulting in large differences between the simulated and experimental sieving rate. Here, a mesh-type, 3D woven structure was accurately modeled, and the simulated sieving process yielded results more closely resembling the experimental process. The woven-mesh model constructed of sine and cosine functions was also used to assess the effect of the structures on the sieving rate and mesh-blocking phenomena, i.e., cohesionless particles plugging the mesh. By monitoring the in situ blocking conditions in the discrete-element method simulation, cohesionless particles with diameters of 1.1w (where w is the size of the aperture) were found to block the most mesh apertures. The large difference in sieving rates observed when separating particles with sizes of 0.7w and 1.1w and those of 0.9w and 1.1w resulted from the differing degree of freedom for the smaller particles to move to the bottom of the bed. The 0.7w particles were more able to move downward in the bed and be sieved out, leading to a higher sieving rate as compared to those with 0.9w diameters. The significant factors and phenomena of the sieving process, such as particle–mesh and particle–particle interactions, instantaneous mesh-blocking, and the intrinsic motion of the granular bed, which cannot be observed experimentally, can be modeled by the DEM simulation using our 3D woven-mesh model. © 2010 American Institute of Chemical Engineers *AIChE J,* 57: 918–928, 2011
Keywords: DEM, sieving, woven mesh, vibration, granular bed

Correspondence concerning this article should be addressed to K. L. Tung at kuolun@cycu.edu.tw.

Introduction

Granular materials display various properties during processing, such as dispersion, fluidization, bridging, aggregation,

and heaping, depending on the operating system, which results in difficulties in controlling bulk behavior. The treatment processes for granular materials, including separation[1–5] or mixing[6] of particulate sizes, transportation in a tube,[7,8] leaking in a hopper, filtration through a screen, etc., have played vital roles in chemical-engineering industries. Among them, screening is used to separate granular materials of different sizes by oscillating the mixture on a mesh and includes most of the above phenomena, making this worthy of study. To better understand the screening process, the granular bed motion in a vibrating system and the effect of the mesh structure should be known.

The granular bed motion in a vibrating system is determined by many factors, such as vibratory amplitude, vibratory frequency, particle size, bed scale, and so on. The mechanism of the motion involves many obscure physical phenomena, such as interior convection[9–16] and diverse motions of particles in the granular bed,[17,18] so study of the bed-motion mechanism has drawn much research attention. For example, Jaeger and Nagel[19] thoroughly reviewed the mechanistic studies of the bed motion in 1992. To experimentally assess the interior motion of a granular bed, for convenience, a two-dimensional vibration system composed of two parallel transparent plates separated by a granular bed only one layer thick has often been utilized for the observation of particle migrations. It is interesting that the larger particles tend to migrate upward and the smaller ones tend to move downward after a period of oscillation. The mechanisms of mixing and separation are affected by interior convection and the width of the bed.[14] However, the two-dimensional system may neglect some significant factors, such as the 3D space and the wall effect. Thus, magnetic resonance imaging technology has been further applied to investigate the particle motion of the vibrating bed.[20–22] To reduce experimental costs and improve the observation of the particle motion in the bed, discrete-element method (DEM) simulations were developed to observe the instantaneous phenomena and analyze important factors that cannot easily be studied experimentally,[8,23–26] such as the particle velocity, the height of the bed, and the particle–mesh interaction. In the past, some researchers have attempted to analyze the screening results of the experiments to predict the screening efficiency via analogy methods,[27] probability statistics,[28] kinetic models,[29] and exponential function trends.[30] However, it has proven difficult to obtain several parameters for the granular motion, such as the particle velocity, the height of the bed, and the particle–mesh interaction, by the above four methods. Therefore, Shimosaka et al.[24] estimated the sieving rate of powders using a custom-made bead-mesh structure with a computer simulation and compared the simulation results with an experimental vibratory sieving process using a woven JIS testing sieve. The predictions of the sieving process by the simulation were expected to differ from the experiment due to differences in the mesh structures, i.e., bead for simulation and woven for the experiment. Simplified mesh structures, such as the bead structure, have been applied in computational simulations[24,31,32] due to the complexity of woven structures. In addition, the particle-mesh interaction, a significant factor in the sieving process, is also dependent on the mesh structures, with the plugging particles having diameters of 1–1.2w. Therefore, an accurate simulated mesh structure is an important factor for obtaining accurate predictions for the sieving process.

In this study, a 3D woven-mesh model constructed of sine and cosine functions was used to predict sieving experiments via the DEM. The results predicted for the sieving rate by the custom-made woven-mesh structure model were very close to the experimental results. The effect of the different mesh structures on the sieving rate, such as plate, bead, and woven mesh, was also studied in this work. Particle-mesh interactions were clearly observed in the DEM simulation over the studied vibration time, where plugging particles with diameters of 1.1w blocked the most mesh apertures, while the particles with 1.3w diameters did not block the apertures. Through the purpose-built DEM simulation in this work, more phenomena and parameters that cannot be obtained experimentally can be studied to further elucidate the sieving process.

Materials and Methods

DEM theory

The discrete-element method was developed by Cundall and Stack[33] to simulate the pressure variation in two-dimensional (2D) soil systems by calculating the dashpot force and elastic force among the soil particles interactively. Tsuji et al.[8] combined the DEM with the Hertzian contact theory to simulate the transport situation in a horizontal straight tube and extended it to a fluidized bed, known as a multiphase system.

The DEM model is based on Newton's laws of motion. When two spherical particles i and j come in contact, which can be determined by the occurrence of an overlap, δ, between them (Figure 1), the interaction forces f in the normal and tangential directions at a time t are described by Eqs. 1 and 2:

$$[f_n]_t = [e_n]_t + [d_n]_t \tag{1}$$

$$[f_s]_t = [e_s]_t + [d_s]_t \tag{2}$$

where the suffix n represents the normal direction and s indicates the tangential direction, and e and d are the elastic force and dashpot force, respectively. In addition, the variations in elastic forces over a very short time are given by Eqs. 3 and 4;

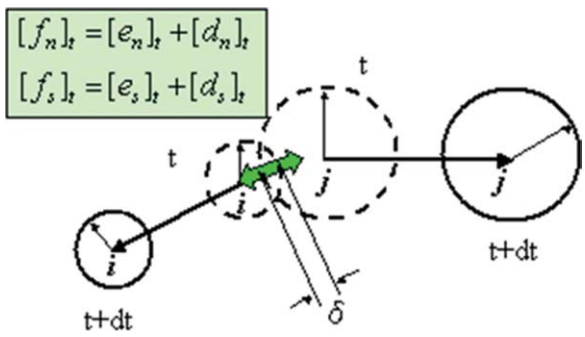

Figure 1. The soft spherical model.

[Color figure can be viewed in the online issue, which is available at wileyonlinelibrary.com.]

$$\Delta e_{\mathrm{n}} = K_{\mathrm{n}} \Delta u_{\mathrm{n}}^{3/2} \tag{3}$$

$$\Delta e_{\mathrm{s}} = K_{\mathrm{s}} \Delta u_{\mathrm{s}}^{3/2} \tag{4}$$

Meanwhile, the variations in dashpot forces are described in Eqs. 5 and 6.

$$\Delta d_{\mathrm{n}} = \eta_{\mathrm{n}} \frac{\Delta u_{\mathrm{n}}}{\Delta t} \tag{5}$$

$$\Delta d_{\mathrm{s}} = \eta_{\mathrm{s}} \frac{\Delta u_{\mathrm{s}}}{\Delta t} \tag{6}$$

However, if the normal force exceeds the frictional sliding force $\left|[e_s]_t \geq \mu[e_n]_t\right|$, then

$$\left|[e_{\mathrm{s}}] = \mu[e_{\mathrm{n}}] \times \mathrm{SIGN}([e_{\mathrm{s}}]_{\mathrm{t}})\right|, \text{ or } [d_{\mathrm{s}}]_t = 0.$$

The SIGN will be "+" if $[e_{\mathrm{n}}]_t \geq 0$ or "−" if $[e_{\mathrm{n}}]_t < 0$, indicating the direction opposite to the displacement of the particle.

Furthermore, the force and the moment in the X, Y, and Z directions are given by Eqs. 7–10:

$$[f_x^i]_t = \sum_j \{[f_{\mathrm{n}}]_t n_1 + [f_{\mathrm{s}}]_t n_1\} \tag{7}$$

$$[f_y^i]_t = \sum_j \{[f_{\mathrm{n}}]_t n_2 + [f_{\mathrm{s}}]_t n_2\} \tag{8}$$

$$[f_z^i]_t = \sum_j \{[f_{\mathrm{n}}]_t n_3 + [f_{\mathrm{s}}]_t n_3 + mg\} \tag{9}$$

$$[\tau^i]_t = \sum_j \{r^i \vec{n} \times [f_{\mathrm{s}}]_t\} \tag{10}$$

where r is the radius of the particle and the unit vector, $\vec{n}$, is $[n_1, n_2, n_3]$. After the analysis of forces, the displacements of the particles can be predicted by Eqs. 11–14.

$$[\Delta S_x^i]_t = [v_x^i]_t \Delta t \tag{11}$$

$$[\Delta S_y^i]_t = [v_y^i]_t \Delta t \tag{12}$$

$$[\Delta S_z^i]_t = [v_z^i]_t \Delta t \tag{13}$$

$$[\Delta \theta^i]_t = [\theta^i]_t \Delta t \tag{14}$$

Finally, the trajectories of the particles are found by integrating the displacements over a short time, Δt.

Vibratory screening system setup

The vibratory screening system setup is schemed in Figure 2. The system is a cylindrical column with 0.15 and 0.2 m in height and diameter, respectively. The black and white colors of particles in Figure 2 represent the different particle sizes. Three different mesh structures, plate-, bead-, and woven-mesh, were simulated as the bottom part of the column. The mesh apertures, w, were all 8.5×10^{-3} m in the simulated system. The detailed description of three mesh structures was discussed later. Initially, the different particle sizes of the cohesionless particles were randomly placed and without contacting each other in the column. For the discussion of mesh structure effect, two different particle diameters, 7.0×10^{-3} and 10.5×10^{-3} m, were used. As for the discussion of particle–mesh and particle–particle interaction, four different particle diameters, $0.7w$, $0.9w$, $1.1w$, and $1.3w$, were utilized for comparison. The total numbers of particles were 844 and the number ratio of large to small particles is 2 in both cases.

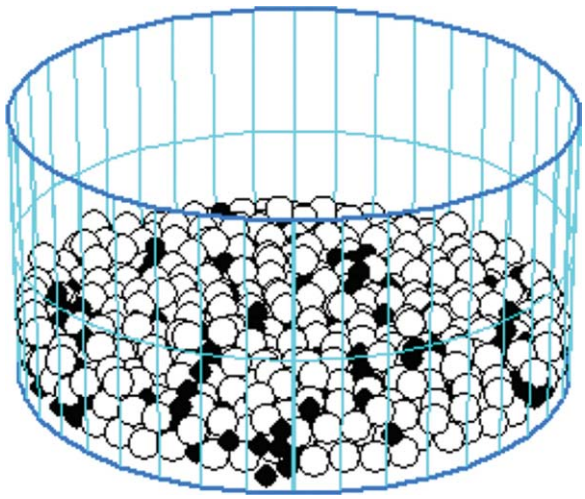

Figure 2. The scheme diagram of 3D vibratory screening system setup.

[Color figure can be viewed in the online issue, which is available at wileyonlinelibrary.com.]

Screening model

In this study, the 3D screening process was simulated by the DEM; a flow chart of the program is shown in Figure 3. In addition, the values of the parameters used in this work are listed in Table 1. Three different mesh structures, plate-, bead-, and woven-mesh structures, as shown in Figure 4, were used to analyze the resulting sieving rate for comparison. The plate mesh was simply built by crisscrossing two sets of rods in the horizontal and vertical directions, as shown in Figure 4a. The results of the bead-mesh system were obtained from a previous study by Shimosaka et al.[24] In addition to the plate- and bead-mesh structures, the structure of the woven mesh shown in Figure 4c was described by Eqs. 15 and 16 in perpendicular directions:

$$\text{Sin type: } Z^f(\kappa) = p \sin(q\kappa) \tag{15}$$

$$\text{Cos type: } Z^f(\kappa) = p \cos(q\kappa) \tag{16}$$

In Eqs. 15 and 16, Z^f represents the Z coordinate of the fiber and κ is the X or Y coordinate of the fiber, whereas p and q are the wave length and wave amplitude, respectively, as shown in Figure 5. Then, the Newton-Raphson method was applied to determine the touch point between the particle and mesh, and the direction of the acting force was calculated.

Results and Discussion

When the depth of the sieving layer is less than six particles, the effects of the mesh structure and the near-mesh-

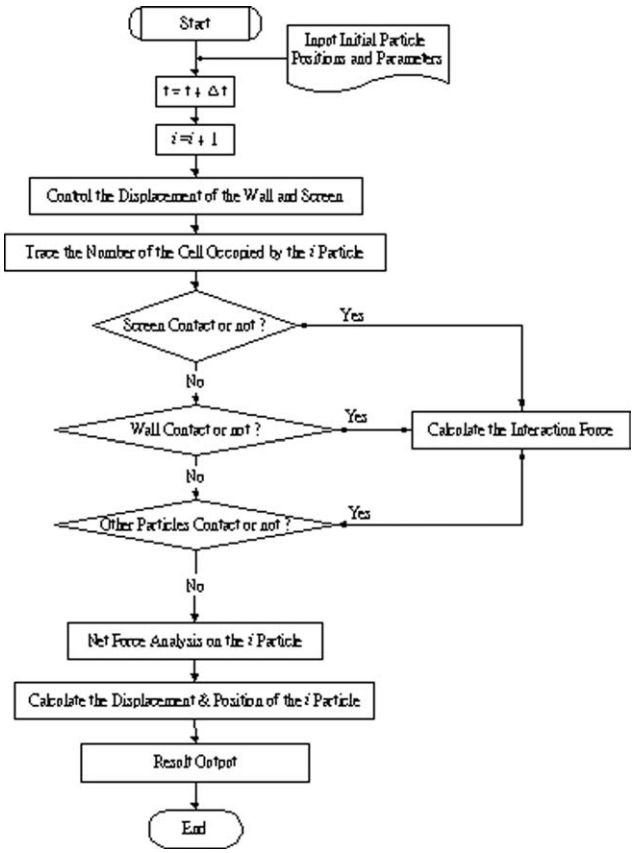

Figure 3. A flow chart of the vibratory process simulation.

sized, or plugging, particles are the two dominant factors in the sieving process. The effect of the mesh structure will be discussed in the effect of the mesh structure section, therefore, the near-mesh-sized particles of 7 and 10.5 mm in diameter and three different mesh structures were used to analyze the effects on the sieving process, respectively. While the interaction between the plugging particles and the mesh will be studied in particle–mesh and particle–particle interaction section. In this section, four different particle diameters, $0.7w$, $0.9w$, $1.1w$, and $1.3w$, simulated woven meshes were utilized to investigate the particle–particle and particle–mesh interaction, respectively.

The effect of the mesh structure

Figure 6 shows the residue–time curve at three different vibration frequencies, 20, 28, and 36 Hz, using the simulated

Table 1. Parameters of the Three-Dimensional System in a Vertical Vibratory Bed

Parameter	Value
Number of particles	844
Particle diameter d_p, m	7.0×10^{-3} and 10.5×10^{-3}
Friction coefficient	
Particle/ particle, f_p	0.5
Particle/ Wall, f_w	0.4663
Particle density ρ, kg/m^3	2.55×10^3
Spring coefficient	
Particle/particle E_p, Pa	6.68×10^7
Particle/wall E_w, Pa	6.68×10^7
Poisson ratio	
Particle/particle, v_p	0.3
Particle/wall, v_w	0.3
Vibratory amplitude A, m	$1.5 \times 10^{-3} - 4.5 \times 10^{-3}$
Mesh aperture w, m	8.50×10^{-3}
Wire gauge d_m, m	2.125×10^{-3}
Time step Δt, s	1.0×10^{-6}

woven- and bead-mesh structures in this work and the previous literature; the sieving experiment was also carried out for comparison in a previous work.[24] The sieving results obtained using the simulated woven-mesh structures agreed very well with the experimental results for all different vibrational frequencies, implying that the construction of the simulated woven-mesh model can be successfully applied to predict the sieving process, as shown in Figure 6. The sieving curve of the residue–time plot can be generally divided into two regions, a high sieving rate at the initial sieving time and a low sieving rate at the later stage. This is clearly observed in the residue–time curves in Figure 6, with regions of high- and low-sieving rates at three different vibrational frequencies. The condition at the vibrational frequency of 36 Hz in Figure 6 reveals the better sieving rate as compared to the other two vibration frequencies of 20 and 28 Hz. Note that the sieving results of the simulated woven-mesh structure are much closer to the experimental results than those of the simulated bead-mesh structures,[24] as shown in Figure 6. Two possible reasons for this result were considered. First, the sizes of the sieving aperture for the simulated woven mesh and the experimental sieve were both 8.5 mm, while that for the simulated bead mesh was 9.6 mm.[24] The larger particles of 10.5 mm in diameter can more easily block the holes of the simulated bead mesh than the simulated woven mesh, resulting in a decrease of sieving rate for the bead mesh. Second, the simulation of the bead mesh by Shimosaka et al.[24] simplified the structures into a web chain using spherical particles of 4.25 mm in diameter, not

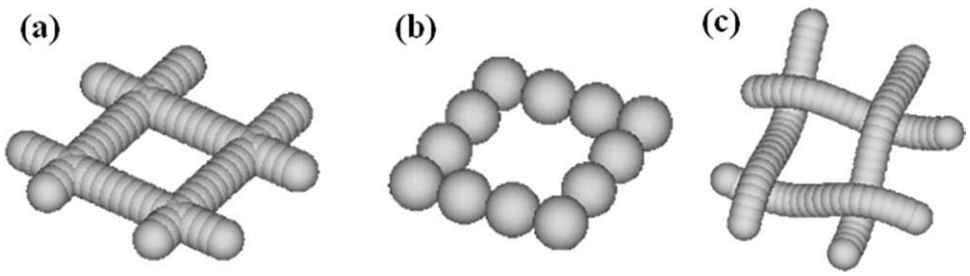

Figure 4. Three kinds of unit mesh apertures; (a) plate mesh, (b) bead mesh, and (c) woven mesh.

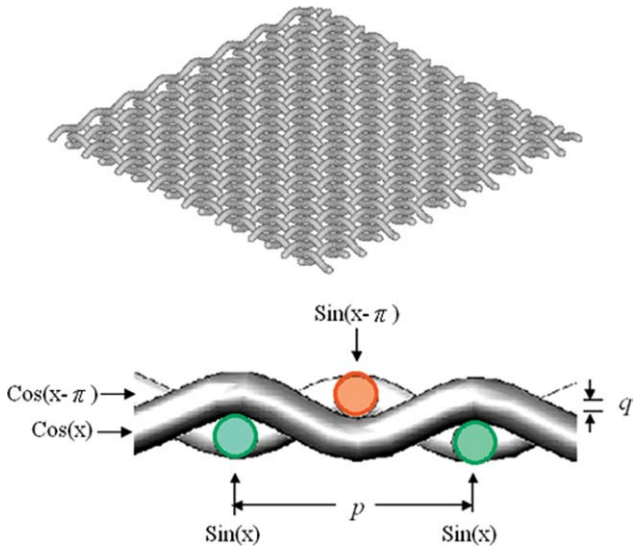

Figure 5. A diagram of the woven-mesh model used in the numerical method.

[Color figure can be viewed in the online issue, which is available at wileyonlinelibrary.com.]

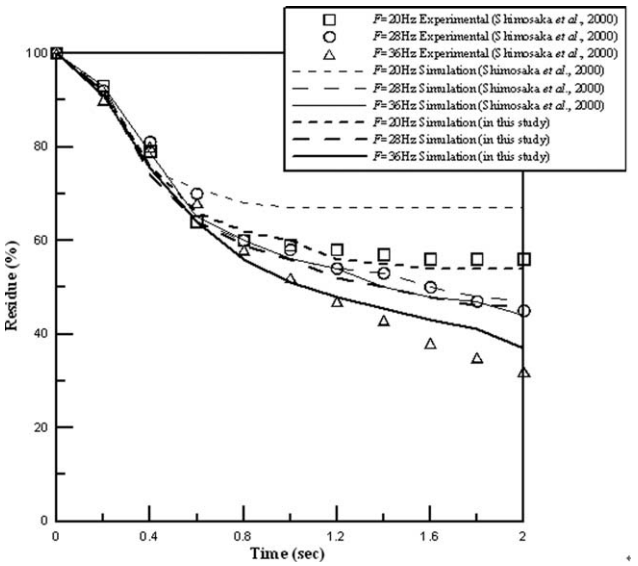

Figure 6. Residue–time curves at the different vibration frequencies with A = 1.5 mm.

completely corresponding with the real sieve mesh. As is readily observed in Figure 6, the residues from the simulations are all higher than those from the respective experiments, leading the model to underestimate the real sieving rate in most cases. This means that the mesh structure is a significant factor in changing the motion of the particles. The larger particles have up to eight contact points when loaded onto the bead mesh,[24] but those on the woven-mesh structure only have four contact points. Therefore, the smaller particles can more easily strike the larger ones on the mesh, possibly resulting in an enhanced separation effect between the particles for the woven-mesh structures. Therefore, the smaller particles may have a greater chance of reaching the bottom layers of the particle bed and being sieved out, leading to the better sieving rate for the simulated woven-mesh structures.

To further discuss the effects of the sieving mesh structures, the simulated plate mesh was also used for comparison at two different vibration frequencies of 20 and 36 Hz, as shown in Figure 7. For the lower vibration frequency of 20 Hz (Figure 7a), the simulated curve of the plate mesh is closer to the experimental curve, as compared to that for the bead mesh, indicating that the sieving rate of the simulated bead mesh would be underestimated when compared with that of the simulated plate mesh at the lower frequency. However, the simulated and experimental sieving results for the plate and bead mesh at the higher vibration frequency of 36 Hz showed the opposite trend, as shown in Figure 7b. For the lower vibration frequency of 20 Hz, the large particles above the plate mesh were more easily moved by the weak oscillation and did not heap upon and block the sieve, so that many small particles could easily reach the lower

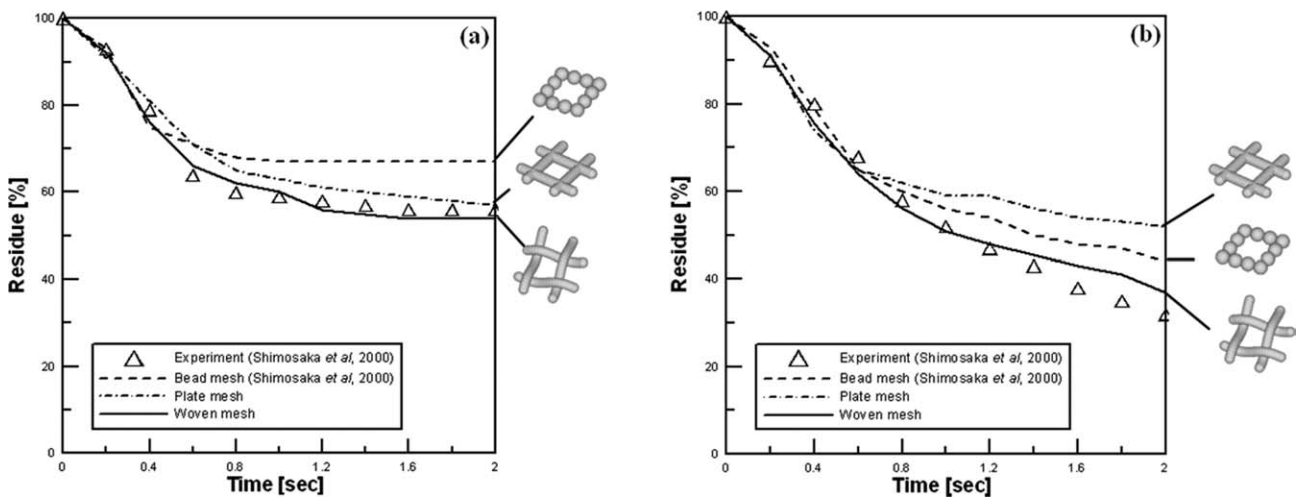

Figure 7. (a) Residue–time curves of the three different kinds of mesh at F = 20 Hz and A = 1.5 mm; (b) residue-time curves of the three different kinds of mesh at F = 36 Hz and A = 1.5 mm.

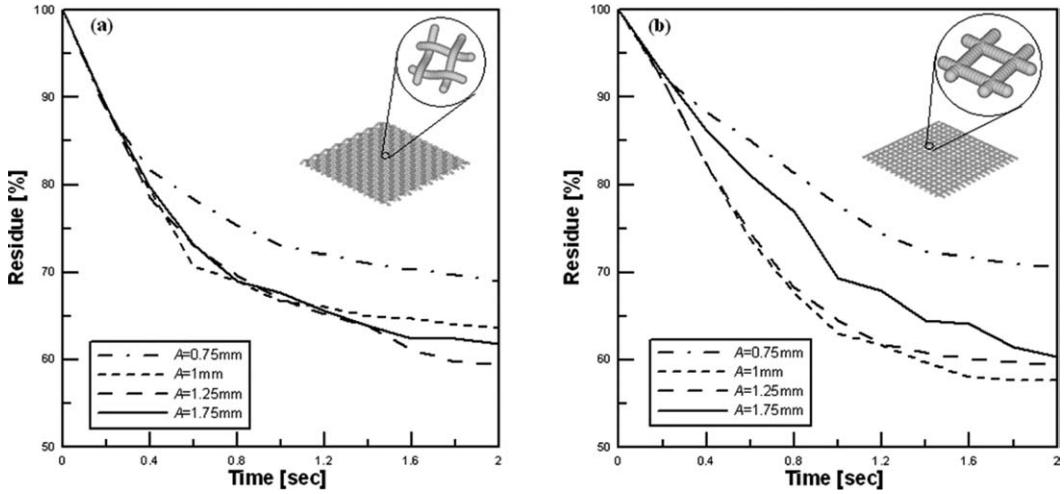

Figure 8. (a) Residue–time curves of four different amplitudes with the woven mesh at $F = 25$ Hz; (b) residue-time curves of four different amplitudes with the plate mesh at $F = 25$ Hz.

layers of the particle bed to pass through the mesh, resulting in a better sieving rate. At the higher vibration frequency of 36 Hz, the steric factor of the bead mesh can provide not only a vertical force but also a horizontal one, pushing the large particles away from the mesh, leading to an increase in the sieving rate for the bead-mesh structures.

Figures 8a,b present the residue–time curves of the woven and plate mesh, respectively, at four different vibration amplitudes. It is obvious that the sieving rate of the woven mesh was higher than that of the plate mesh at the initial stage of the sieving process. This means that when the small particles load onto the cross area of the rough woven mesh, they are in a less stable condition and tend to be sieved out by gravity. Instead, if the small ones load onto the cross area of the smooth plate mesh, the greater upward force causes them to be lifted, rather than to be sieved out. The particle bed will expand, attaining a higher porosity at the initial stage of the sieving process, so most of the small particles are capable of falling and being sieved out. After a while, the porosity of the particle bed decreases and the bed comes to a stable condition. Later, the number of small particles at the bottom of the bed retained on the mesh surface plays a significant role. On the plate mesh, these small particles are less likely to return to the interior of the bed due to crowding, and this improves their chance of falling through the sieve. As a result, the sieving rate was higher for the plate mesh. The rougher surface of the woven mesh encouraged the small particles at the bottom to reinvade the crowded granular bed, resulting in a layer rearrangement of the bed. This increased the chance of small particles returning to the bed and reduced the sieving rate. Therefore, the sieving rate of the plate mesh was higher than that of the woven one at the later stage of the sieving process. In addition, it can be clearly observed that the sieving rate was increased as the vibration amplitude was increased from the lowest vibration amplitude, but when it was increased beyond a certain value, the sieving ability declined, implying that there is an optimum value of the vibration amplitude with respect to the sieving rate; the values were 1.25 and 1 mm for the woven- and plate-mesh systems, respectively. In other words, the lowest residues at the last vibration time of 2 s were at the vibration amplitudes of 1.25 and 1 mm as illustrated in Figures 8a, b, implying the better sieving rate for these two amplitudes, respectively. Both vibration amplitudes of 1.25 and 1 mm were not the largest amplitude values in the woven- and plate-mesh systems, respectively; therefore, there is an optimum value of the vibration amplitude with respect to the sieving rate.

The motion of the particles in the granular bed was also analyzed from a microscopic viewpoint using the constructed simulation method, examining factors such as the relative velocities of two different sizes of bed particles, which cannot be observed experimentally. The relative velocities define as the velocity difference between the large and small particles. Figures 9a–d display the plots of the relative velocities for the large and small particles and the vibration times at four different vibration amplitudes using the simulated woven meshes. A positive relative velocity means that the large particles move upward sooner than the small ones, implying a better separation between large and small particles, while the small ones stay at the bottom of the granular bed. Therefore, larger relative velocities represent a better sieving rate. As shown in Figures 9a–d, the largest relative velocities were located around 0 to 0.4 s, leading to the higher sieving rate for the larger vibration amplitudes at the initial stage of the sieving process, which corresponds to the results of Figure 8a. This suggests that the small particles were mainly sieved out through the granular bed at the initial stage of the sieving process. After carefully observing the results for vibration times from 0.2 to 0.6 s in Figure 9, the smallest relative velocity is observed at the vibration amplitude of 0.75 mm, resulting in a lower sieving rate when compared with the other vibration amplitudes, which also agrees with the results of Figure 8a. During the vibration time from 1.2 to 2 s, the relative velocity at the vibration amplitude of 0.75 mm is larger than that at 1 mm, indicating that the sieving rate at the vibration amplitude of 0.75 mm was higher than that of 1 mm, which is the same as in the results of Figure 8a. However, the largest relative velocities, at vibration amplitudes of 1.25 and 1.75 mm, indicated the highest sieving rate among these four vibration amplitudes.

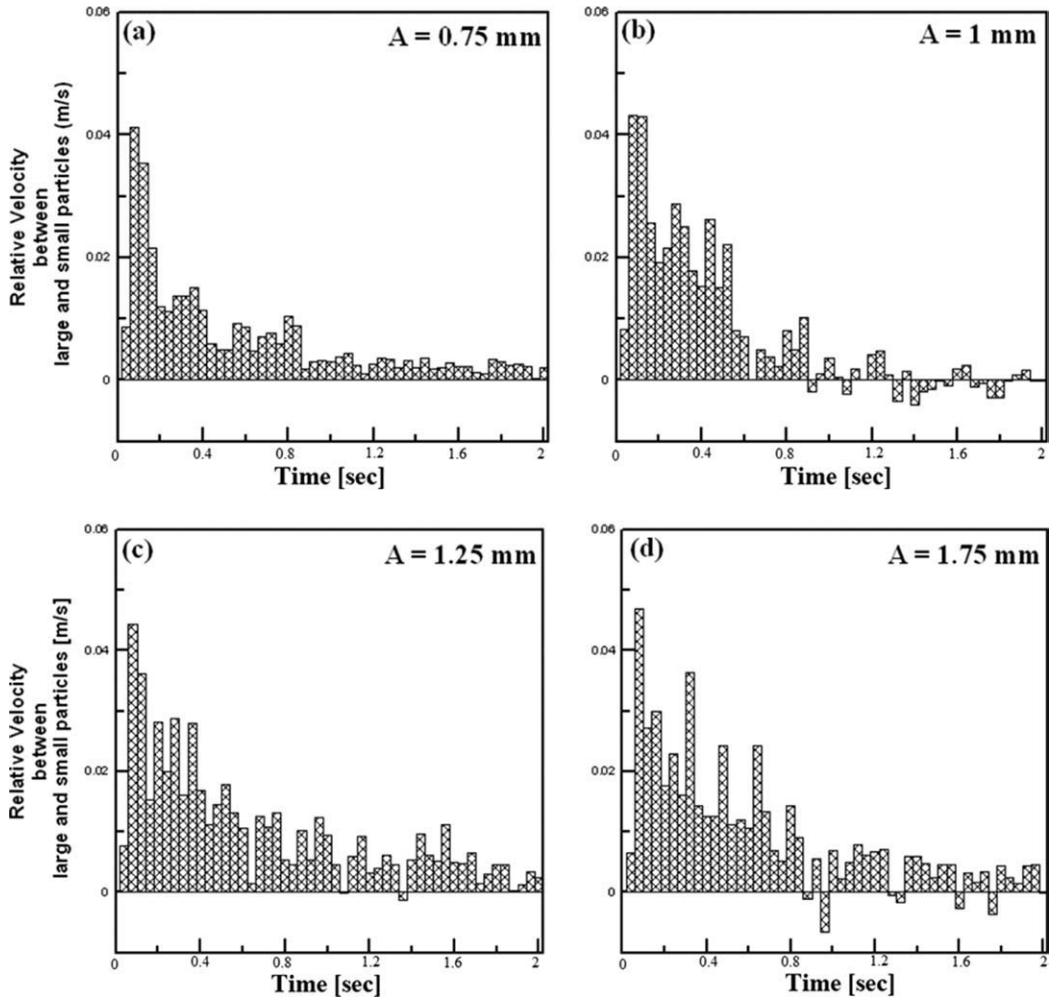

Figure 9. The average velocity of large particles relative to small particles at $F = 25$ Hz for amplitudes of (a) 0.75 mm, (b) 1 mm, (c) 1.25 mm, and (d) 1.75 mm.

Based on the above results, the larger relative velocities imply a higher degree of separation of large and small particles, which assists in the sieving process. It should be noted that the condition that the sieving rate at the vibration amplitude of 0.75 mm was higher than that of 1 mm is only for the vibration time from 1.2 to 2 s, instead of the final vibration screening process. The custom simulation method in this work allowed for a clear observation of phenomena from a microscopic viewpoint, which is not possible experimentally.

Particle–mesh and particle–particle interactions

From the viewpoint of the interaction between particles and the mesh aperture of the woven mesh, the particles with sizes between $1.0w$ and $1.2w$ (where w is the mesh aperture), the so-called plugging particles, will decrease the sieving of small particles due to mesh-blocking by the larger ones. To evaluate the blocking effect of plugging particles, the sieving rate of four different particle-size combinations, $0.7w$ and $1.1w$, $0.9w$ and $1.1w$, $0.7w$ and $1.3w$, and $0.9w$ and $1.3w$, were modeled, and the results are shown in Figure 10. Here, the sieving rate of the $0.9w/1.1w$ and $0.7w/1.1w$ pairs were both lower than the other two cases due to the $1.1w$-diameter

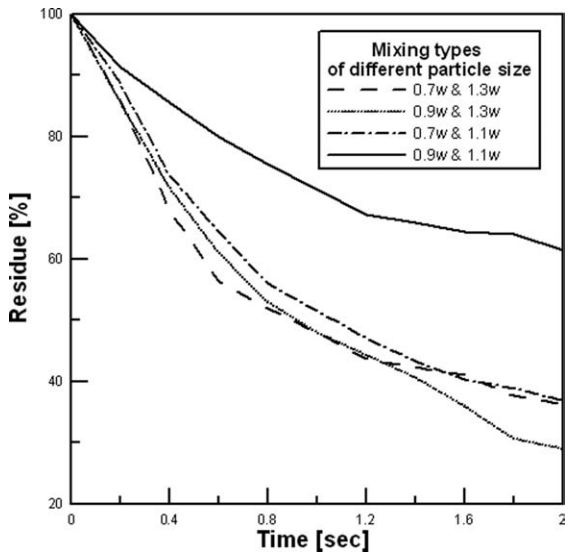

Figure 10. Residue–time curves of different particle–size combinations at $F = 28$ Hz and $A = 1.5$ mm.

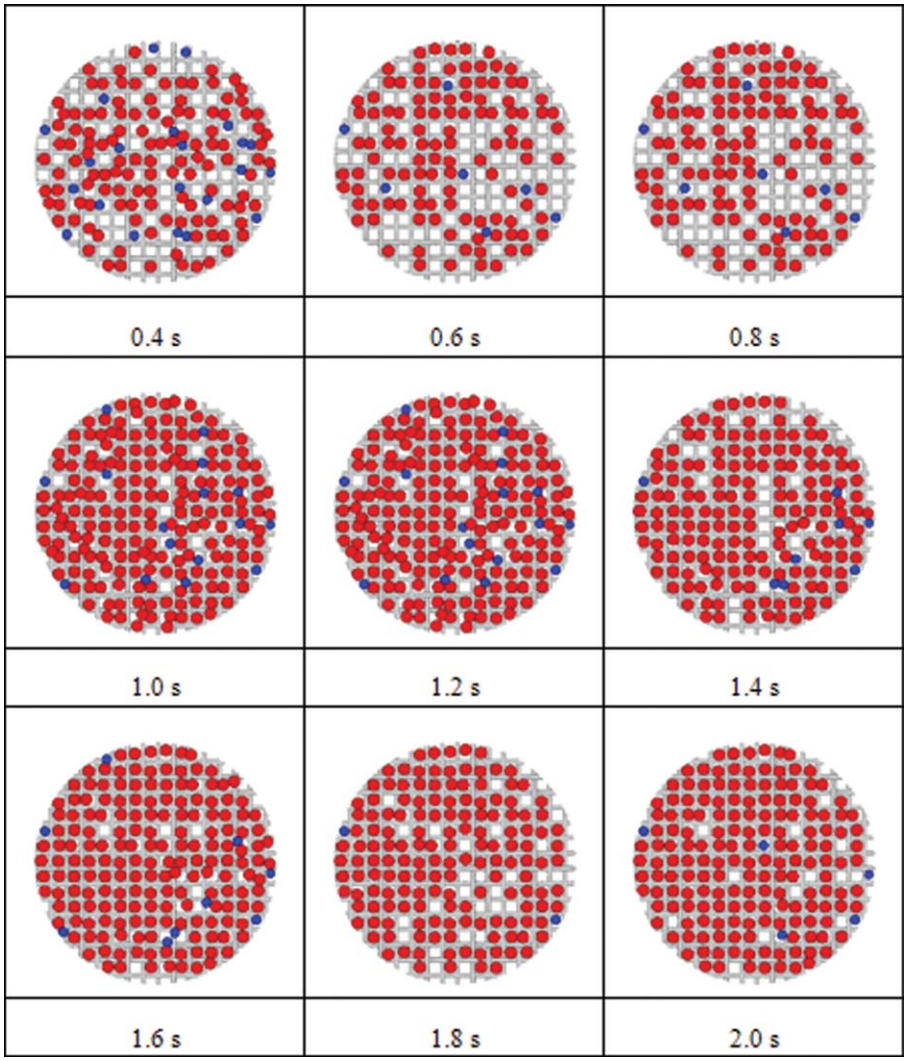

Figure 11. The mesh-blocking condition for the particle sizes of 0.9*w* and 1.1*w* from 0.4 to 2 s.

[Color figure can be viewed in the online issue, which is available at wileyonlinelibrary.com.]

plugging particles. However, the case of 0.7*w*/1.1*w* had a sieving rate closer to that of the 0.7*w*/1.3*w* and 0.9*w*/1.3*w* pairs, while the case of 0.9*w*/1.1*w* had a much lower sieving rate than the other three cases. To clarify the above issues, the numerical simulation was helpful in investigating aspects that cannot be studied experimentally. The in situ blocking conditions between the mesh and particles with sizes of 1.1*w* and 1.3*w* were performed every 0.2 s via simulation processes, as shown in Figures 11 and 12, respectively. In Figure 11, the 1.1*w* particles perpetually occupy most of the apertures after a time, while the 1.3*w* particles only block the aperture temporarily and tend to migrate with the lasting oscillation, as shown in Figure 12. The above result clearly indicates that the plugging particles, in this case with a size of 1.1*w*, decrease the sieving ability of the smaller particles, due to their blocking of the mesh apertures. Figure 13 illustrates the plot of the mesh blocking rate vs. time for the two cases of 0.7*w*/1.1*w* and 0.9*w*/1.1*w*, revealing that the two cases had similar blocking conditions between the plugging particles (here both 1.1*w*) and the mesh. Therefore, we wondered what the significant factor for the large difference in the sieving rates of the two cases (0.7*w*/1.1*w* and 0.9*w*/1.1*w*) might be, aside from the effect of the aperture blocking. For a typical sieving process, the ability of the smaller particles to move down in the granular bed and be sieved out is very important for the sieving rate. The higher mobility of smaller particles toward the bottom of the bed provides more chances to be sieved out, leading to an increase in the sieving rate. Therefore, the percentages of the smaller particles moving to the bottom of the bed with different combinations of particle sizes, 0.7*w* and 1.3*w*, 0.7*w* and 1.1*w*, and 0.9*w* and 1.1*w*, were studied by recording the locations of the smaller particles using the simulation method, as shown in Table 2. The case of 0.9*w*/1.1*w* had the lowest percentage value of 3%, indicating that the probability of the smaller particles moving to the bottom of the bed was very small. In consequence, the higher mobility of the small particles in the case of 0.7*w*/1.1*w* as compared to that of 0.9*w*/1.1*w* resulted in a higher sieving rate in spite of the same mesh-blocking effect of the plugging particles, 1.1*w* in both cases. To further

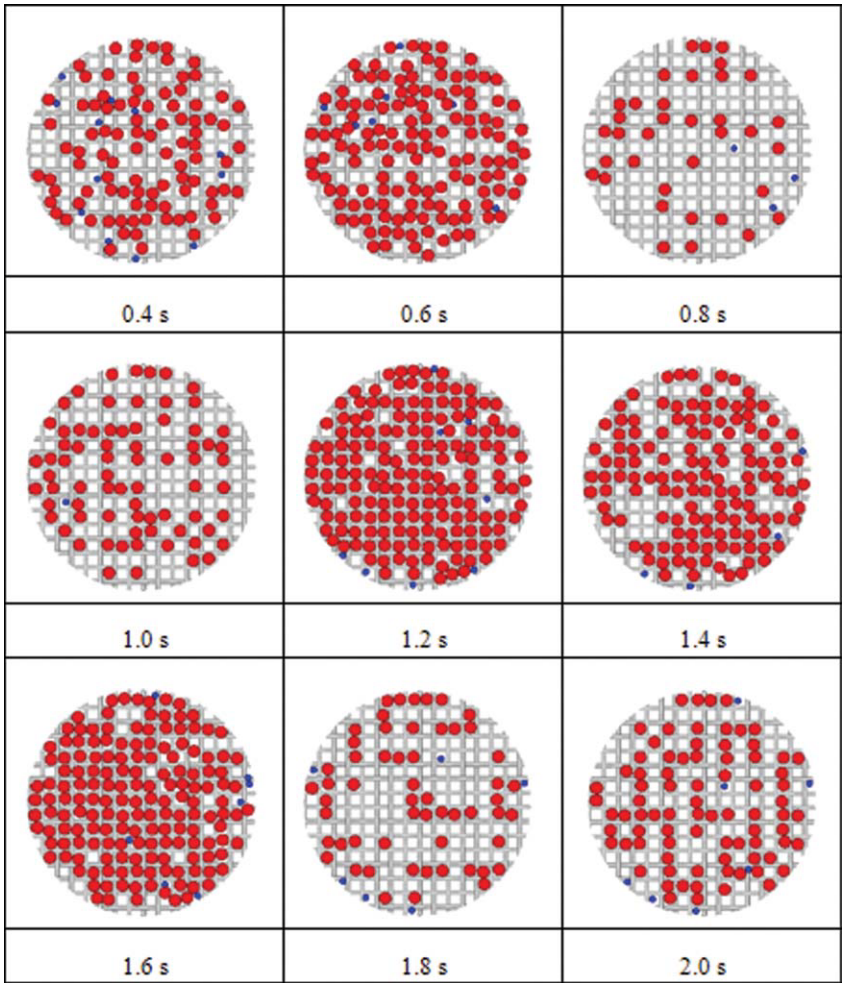

Figure 12. The mesh-blocking condition for the particle sizes of 0.9*w* and 1.3*w* from 0.4 to 2 s.

[Color figure can be viewed in the online issue, which is available at wileyonlinelibrary.com.]

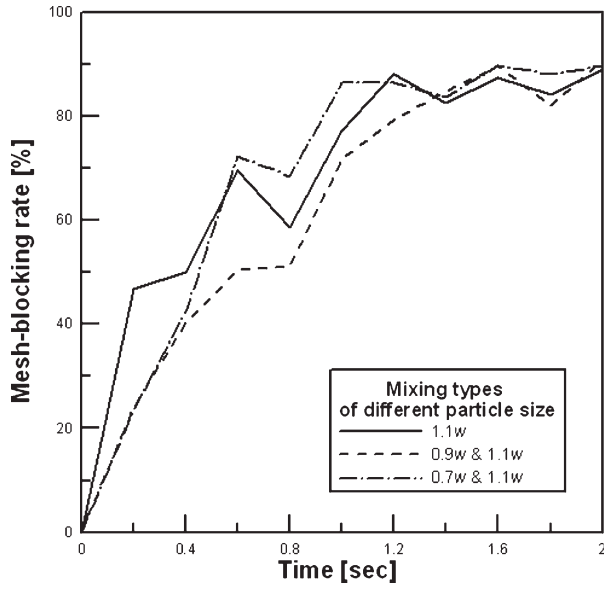

Figure 13. Plot of the mesh-blocking percentage vs. the sieving time at *F* = 28 Hz and *A* = 1.5 mm.

Table 2. Percentage of Small Particles Moving to the Bottom of the Bed for Different Combinations of Particle Sizes

Particle Sizes	Percentage of Small Particles Moving to the Bottom of the Bed (%)
0.7 and 1.3*w*	50
0.7 and 1.1*w*	27
0.9 and 1.1*w*	3

confirm the effect of the mobility of the small particles on the sieving rate in these two cases, the system was reset into two opposite initial sieving situations. In the first, all of the smaller particles were initially set above the granular bed, as shown in Figure 14, while in the other, they were all set under the bed, as shown in Figure 15. For the first case, the sieving rate of the 0.9*w*/1.1*w* system suddenly decreased to a very small value as compared to the 0.7*w*/1.1*w* system, indicating that the smaller particles in the 0.7*w*/1.1*w* pair have better mobility than those in the 0.9*w*/1.1*w* pair. For the case of the smaller particles initially placed at the bottom of the bed, the sieving rate of the 0.9*w*/1.1*w* pair increased immediately, reaching the same order of magnitude as for the 0.7*w*/1.1*w* pair, reflecting

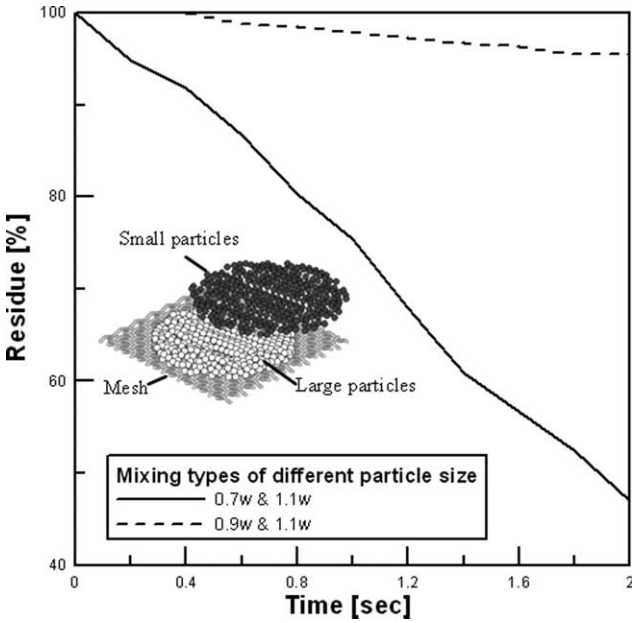

Figure 14. Residue–time curve for the case in which the smaller particles are initially set in the upper layer of the bed at F = 28 Hz and A = 1.5 mm.

the increased chance for the small particles to be at the bottom of the bed for the case of the 0.9w/1.1w system (Figure 15). The above results reveal that both the aperture-blocking effect by the plugging particles and the mobility of the smaller particles are important factors in the sieving process.

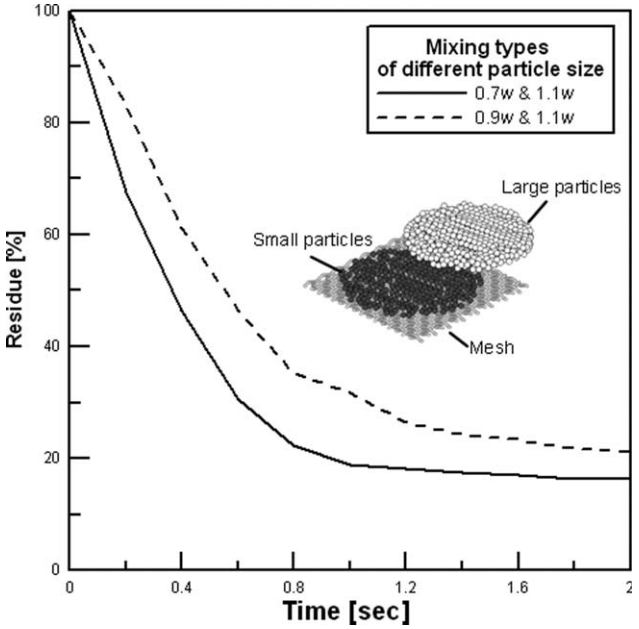

Figure 15. Residue–time curve for the case in which the smaller particles are initially set in the bottom layer of the bed at F = 28 Hz and A = 1.5 mm.

Conclusions

In this study, the discrete-element method was applied to the simulation of a vibratory sieving process. To yield a more realistic understanding of the sieving process, here, a model of a 3D woven-mesh structure was constructed to analyze the particle–mesh interaction of the sieving process, representing an improvement upon the existing 2D bead-mesh structure model. The simulation results of the sieving process using the 3D woven-mesh model were in good agreement with the experimental results by Shimosaka et al.[24] and were better than those of the simplified structural mesh models, such as bead- and plate-mesh structures. Therefore, the 3D woven-mesh model constructed in this work is suitable for prediction of the sieving process in the real world. The significant factors of the sieving process, such as the particle–mesh and particle–particle interactions, were also correctly characterized using our 3D woven-mesh model. The results revealed that the lowest sieving rate occurred for the particle-size combination of 0.9w and 1.1w due to aperture blocking by the 1.1w-diameter plugging particles. The in situ blocking conditions between the mesh and particles with diameters of 1.1w and 1.3w were also monitored by the custom DEM simulation. The particles with diameters of 1.1w were found to block most apertures of the mesh after a time, but the particles with diameters of 1.3w did not, resulting in a decrease in sieving rate for the particles 1.1w in diameter. However, in spite of the existence of the 1.1w plugging particles, the case of 0.7w/1.1w had a sieving rate comparable to that of the 0.7w/1.3w and 0.9w/1.3w pairs, but higher than that of the 0.9w/1.1w pair. The mobility of small particles can account for the above phenomenon, as shown by the DEM simulation. The case of 0.7w/1.1w had a better mobility for smaller particles toward the bottom of the bed than that of 0.9w/1.1w, providing a greater chance for the small particles to pass through the aperture of the mesh, which was clearly observed in our simulation. Therefore, a simulation employing the purpose-built woven-mesh model in this work can be effectively used to predict the sieving process in real-world applications, such as food processing, agriculture, and pharmacy, and to elucidate the significant factors for sieving rate.

Acknowledgments

The authors thank the Center-of-Excellence (COE) Program on Membrane Technology from the Ministry of Education (MOE), R.O.C.; the Distinctive Research Area project of Toward Sustainable Green Technology from Chung Yuan Christian University (CYCU), R.O.C., as grant CYCU-98-CR-CE; and the National Science Council (NSC), R.O.C., for their financial supports.

Notation

Roman

A = vibrational amplitude, m
D = dashpot force, N
E = Young's modulus, Pa
E = spring force, N
F = contact force, N
F = vibrational frequency, Hz
K = Stiffness, N/m
S = displacement of a particle, m
u = relative displacement between two particles, m

v = velocity of a particle, m/s
r = particle radius, m
w = the size of the aperture, m

Greek letters

θ = angular displacement, °
ρ = particle density, kg/m^3
v = Poisson ratio
η = dash-pot coefficient, N s/m

Superscripts

i = reference particle
f = woven screen

Suffixes

n = normal direction
s = tangential direction
$[\ ]_t$ = at time t

Literature Cited

1. Hsiau SS, Wang PC, Tai CH. Convection Cells and Segregation in a Vibrated Granular Bed. *AIChE J*. 2002;48:1430–1438.
2. Hsiau SS, Chen WC. Density effect of binary mixtures on the segregation process in a vertical shaker. *Adv Powder Technol*. 2002; 13:301–315.
3. Arntz MMHD, Otter WK, Briels WJ, Bussmann PJT. Granular mixing and segregation in a horizontal rotating drum: a simulation study on the impact of rotational speed and fill level. *AIChE J*. 2008; 54:3133–3146.
4. Hsiau SS, Yu HY. Segregation phenomena in a shaker. *Powder Technol*. 1997;93:83–88.
5. Rosato AD, Blackmore DL, Zhang N, Lan Y. A perspective on vibration-induced size segregation of granular materials. *Chem Eng Sci*. 2002;57:265–275.
6. Hunt ML, Hsiau SS, Hong KT. Particle mixing and volumetric expansion in a vibrated granular bed. *J Fluids Eng*. 1994;116:785–791.
7. Tsuji Y, Morikawa Y. LDV Measurements of Air-Solid Two-Phase Flow in a Horizontal Pipe. *J Fluid Mech*. 1982;120:385–409.
8. Tsuji Y, Tanaka T, Ishida T. Langrangian numerical Simulation of plug flow of cohesionless pipe. *Powder Technol*. 1992;71:239–250.
9. Hsiau SS, Chen CH. Granular convection cells in a vertical shaker. *Powder Technol*. 2000;111:210–217.
10. Savage SB, Dai R, editors. Some aspect of bounded and unbounded shear flows of granular material. *Advances in Micromechanics of Granular Material*. Potsdam: Elsevier, 1991.
11. Taguchi Y. New origin of convective motion: elastically induced convection in granular materials. *Phys Rev Lett*. 1992;69:1367–1370.
12. Gallas JAC, Herrmann HJ, Sokolowski S. Convection cells in vibrating granular media. *Phys Rev Lett*. 1992;69:1371–1373.
13. Knight JB, Frandrich CG, Lau CN, Jaeger HM, Nagel SR. Density relaxation in a vibrated granular materials. *Phys Rev E*. 1995;51:3957–3963.
14. Lan Y, Rosato AD. Convection related phenomena in vibrated granular beds. *Phys Fluids*. 1997;9:3615–3624.
15. Aoki KM, Akiyama T. Control parameter in granular convection. *Phys Rev E* 1998;58:4629–4637.
16. Yang SC, Hsiau SS. Simulation study of the convection cells in a vibrated granular bed. *Chem Eng Sci*. 2000;55:3627–3637.
17. Hsiau SS, Pan SJ. Motion state transitions in a vibrated granular bed. *Powder Technol*. 1998;96:219–226.
18. Wassgren CR, Brennen CE, Hunt ML. Vertical vibration of a deep bed of granular material in a container. *J Appl Mech*. 1996;63:712–719.
19. Jaeger HM, Nagel SR. Physics of the granular state. *Science*. 1992;255:1523–1531.
20. Altobelli SA. Velocity and concentration measurements. *J Rheol*. 1991;35:721–734.
21. Nakagawa M, Altobelli SA. Non-invasive measurements of granular flows by magnetic resonance imaging. *Exp Fluids*. 1993;16:54–60.
22. Ehrichs EE, Jaeger HM. Granular convection observed by magnetic resonance imaging. *Science*. 1995;267:1632–1634
23. Li J, Webb C, Campbell GM. Discrete particle motion on sieves - a numerical study using the DEM simulation. *Powder Technol*. 2003;133:190–202.
24. Shimosaka A, Higashihara S, Hidaka J. Estimate of the sieving rate of powders using computer simulation. *Adv Powder Technol*. 2000;11:487–502.
25. Sudah OS, Arratia PE, Alexander A, Muzzio FJ. Simulation and experiments of mixing and segregation in a tote blender. *AIChE J*. 2005;51:836–844.
26. Zhu K, Wong CK, Rao SM, Wang CH. Pneumatic conveying of granular solids in horizontal and inclined pipes. *AIChE J*. 2004;50:1729–1745.
27. Beenken W. Method for the mathematical modelling of the screening process on circular vibrating screens. *Aufber Tech*. 1990;31:147–156.
28. Coppers M. Ultraschallsiebung, Dissertation an der Uni- versität Gesamthochschule *Essen*. Aachen: Shaker Verlag, 1997.
29. English JE. A new approach to the theoretical treatment of the mechanics of sieving and screening. *Filtr Sep*. 1974;11:195–203.
30. Andrejczak P, Wodzinski P. Model of screening in the layer. *Powder Handling Process*. 1994;6:263–272.
31. Castro J, Ostoja-Starzewski M. Particle sieving in a random fiber network. *Appl Math Modeling*. 2000;24:523–534.
32. Alkhaldi H, Ergenzinger C, Fleibner F, Eberhard P. Comparison between two different mesh descriptions used for simulation of sieving processes. *Granular Matter*. 2008;10:223–229.
33. Cundall PA, Strack ODL. A discrete numerical model for granular assemblies. *Géotechnique*. 1979;29:47–59.

Manuscript received Oct. 21, 2009, and revision received Mar. 19, 2010.